

Micromorphology of pineal gland calcification in age-related neurodegenerative diseases

Inna Bukreeva¹ | Olga Junemann^{2,1} | Alessia Cedola¹ | Francesco Brun³ |
 Elena Longo⁴ | Giuliana Tromba⁴ | Fabian Wilde⁵ | Marina V. Chukalina^{6,7} |
 Yuri S. Krivonosov⁶ | Irina G. Dyachkova⁶ | Alexey V. Buzmakov⁶ |
 Denis A. Zolotov⁶ | Francesca Palermo¹ | Giuseppe Gigli⁸ | Dmitry A. Otlyga² |
 Sergey V. Saveliev² | Michela Fratini^{1,9} | Victor E. Asadchikov⁶

¹Institute of Nanotechnology – CNR, Rome unit, Rome, Italy

²Research Institute of Human Morphology, Moscow, Russian Federation

³Department of Engineering and Architecture, University of Trieste, Trieste, Italy

⁴Elettra-Sincrotrone Trieste S.C.p.A., Basovizza, Trieste, Italy

⁵Institute of Materials Physics, Helmholtz-Zentrum Hereon, Geesthacht, Germany

⁶Federal Scientific Research Center “Crystallography and Photonics” RAS, Moscow, Russian Federation

⁷Smart Engines Service LLC, Moscow, Russian Federation

⁸Institute of Nanotechnology – CNR, c/o Campus Ecotekne – Università del Salento via Monteroni, Lecce, Italy

⁹Laboratory of Neurophysics and Neuroimaging (NaN), IRCCS Santa Lucia Foundation, Rome, Italy

Correspondence

Inna Bukreeva, Institute of Nanotechnology – CNR, Rome Unit, Piazzale Aldo Moro 5, 00185 Rome, Italy.
 Email: inna.bukreeva@cnr.it

Abstract

Background: The formation of concrements in human pineal gland (PG) is a physiological process and, according to many researchers, is associated with the involution of PG structures. The majority of scientific publications concern progressive calcification of PG, leaving out studies on the destruction of already formed calcified concrements. Our study fills the gap in knowledge about calcified zones destruction in PG in normal aging and neuropathological conditions, which has not been addressed until now.

Purpose: Our objective is to gain insight into human PG tissue impairment in both normal aging and neurodegenerative conditions. X-ray phase-contrast tomography (XPCT) allowed us to study PG tissue degeneration at high spatial resolution and, for the first time, to examine the damaged PG concrements in detail. Our research finding could potentially enhance the understanding of the PG involvement in the process of aging as well as in Alzheimer’s disease (AD) and vascular dementia (VD).

Methods: The research was carried out on human PG autopsy material in normal aging, VD, and AD conditions. Laboratory-based micro-computed tomography (micro-CT) was used to collect and evaluate samples of native, uncut, and unstained PG with different degrees of pineal calcification. The detailed high-resolution 3D images of the selected PGs were produced using synchrotron-based XPCT. Histology and immunohistochemistry of soft PG tissue confirmed XPCT results.

Results: We performed via micro-CT the evaluation of the morphometric parameters of PG such as total sample volume, calcified concrements volume, and percentage of concrements in the total volume of the sample. XPCT imaging revealed high-resolution details of age-related PG alteration. In particular, we noted signs of moderate degradation of concrements in some PGs from elderly donors. In addition, our analysis revealed noticeable degenerative change in both concrements and soft tissue of PGs with neuropathology. In particular, we observed a hollow core and separated layers as well as deep ragged cracks in PG concrements of AD and VD samples. In parenchyma of some samples, we detected wide pinealocyte-free fluid-filled areas adjacent to the calcified zones.

Conclusion: The present work provides the basis for future scientific research focused on the dynamic nature of PG calcium deposits and PG soft tissue in normal aging and neurodegenerative diseases.

KEYWORDS

histology, human pineal gland, microtomography, neurodegenerative diseases, X-ray phase-contrast tomography

1 | INTRODUCTION

The pineal gland (PG) (epiphysis) is a part of the epithalamus. This is an asymmetric formation with a volume of about 1 cm³, located in the geometric center of the mammalian brain (Figure 1). One of the functions of the PG is to synthesize the hormone melatonin, which regulates the circadian rhythms of living organisms.¹ Pineal concretions (also called brain sand, corpora arenacea, acervuli, or psammoma bodies) are common findings in PG autopsy material. Concretions in human PG mainly consist of composite hydroxyapatite. In addition, the trace of manganese, magnesium, zinc, iron, strontium, copper, uranium, and yttrium can also be present in the concretions.^{1,2} The formation of concretions in PG is a physiological process^{3,4} and, according to many researchers, is associated with the involution of PG structures.⁵ The number of extracellular formations progressively increases in aging leading to calcium deposits in the form of “layered spheres” of concretions.⁶ According to the literature, PG by the age of 35–40 undergoes degeneration and decreases in volume.^{7,8} However, some researchers reported the age-independent nature of PG calcification.^{9,10} Moreover, other authors wrote that the number of deposits might dynamically vary during life.¹¹ In numerous publications, calcium deposits in PG have been associated with neurodegenerative diseases such as Alzheimer’s disease (AD) and vascular demen-

tia (VD). AD and VD are among the major healthcare problems.¹² They are characterized by progressive cognitive damage, memory loss, and thinking or speech impairment prevalent among elderly people.^{13–17} VD can be accelerated by AD, stroke, and some peripheral diseases. The degree of involvement and damage of the human PG in the development of AD and VD are not fully understood yet. Attempts of different authors to find a correlation between the accumulation of PG concretions and aging,^{18,19} melatonin levels,²⁰ or neurological disorders^{21,22} remain controversial. To date, it is generally accepted that the degree of pineal calcification in people with AD is higher, and PG volume decreases, compared to healthy people.²¹ The accumulation of calcified concretions can lead to hypoxia and death of PG cells and, therefore, to lower melatonin production.

The goal of the present study is the thorough investigation of the morphological features of PG in normal aging and neurodegenerative condition (AD and VD). We intend to analyze the topological arrangement of calcified zones and to investigate the PG soft and calcified tissue degeneration in native uncut unstained postmortem human PGs. Although PG calcification is an active process that can be associated with both concretions formation and destruction, most publications focus exclusively on PG formation and no comprehensive description of PG concretion destruction has been provided yet. Our study fills the gap in knowledge

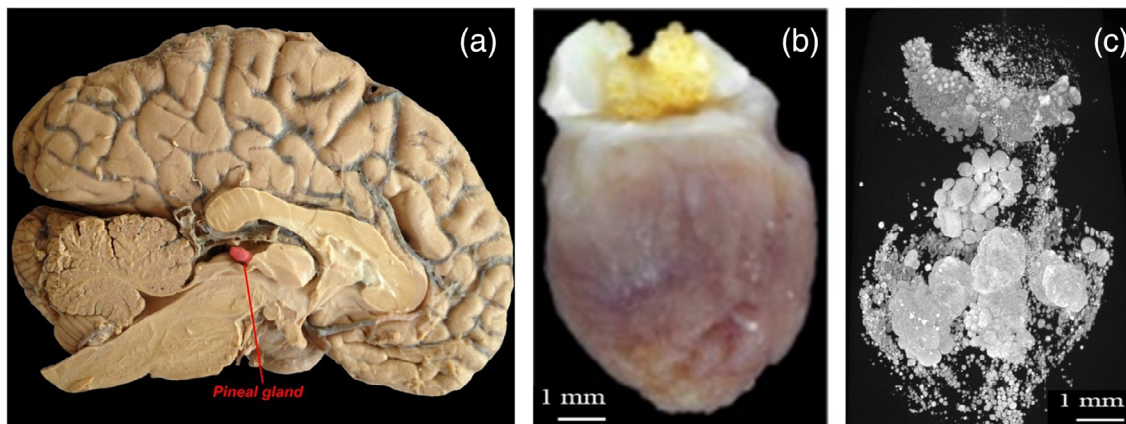


FIGURE 1 (a) Photographic image of the sagittal section of the human brain; (b) human PG; (c) micro-computed tomography (micro-CT) image of a calcified human PG, dense-calcified structures appear white, whereas low-density PG soft tissue is assigned dark color.

about calcified zones destruction in PG in normal aging and neuropathological conditions, which has not been addressed until now.

PG calcification was studied in the literature with histological and histochemical methods,^{23–25} electron transmission, and scanning microscopy²⁶ as well as X-ray micro-computed tomography (micro-CT).²⁷ Histology and immunohistochemistry are the gold-standard imaging techniques used in biomedicine. However, they require a decalcification of hard concretions before cutting PG, which influences the ability of soft tissues to perceive various histological and immunohistochemical staining. Therefore, many researchers prefer methods without the decalcification step, which in turn can lead to concretions destruction. SEM and TEM methods can be used for high-resolution imaging. However, these techniques are destructive and complicated in sample preparation when compared to micro-CT and incompatible with the investigation of large specimens such as massive calcified deposits. X-ray micro-CT is a useful well-established 3D imaging tool that allows noninvasive investigation of the topology and the microstructure of PG concretions. However, it fails in visualizing features which have similar and weak X-ray absorption, for example, PG soft tissue.

X-ray phase-contrast tomography (XPCT) has the potential to overcome these problems.²⁸ The capabilities of XPCT for nondestructive studies of the pineal organ at the level of PG vascular and neural organization and micro-architecture of PG calcification have recently been demonstrated.^{4,29}

In our research, we used micro-CT and propagation-based XPCT imaging (PBI XPCT) setups as relevant noninvasive imaging tools for the 3D investigation of PG. XPCT reconstructed images enabled high-resolution 3D visualization of the whole PG sample with micro-features of the parenchyma and calcification, which could not be detected with other imaging techniques.

Our study via XPCT revealed high-resolution details of age-related PG alteration. In particular, some PGs from elderly donors presented signs of moderate concretions damage such as detachment of layers within concretions and the partial splitting of concretions from calcified conglomerates. In PGs obtained from AD and VD donors, severe degenerative abnormalities such as hollow cores and multiple highly segregated layers were more apparent than in healthy PGs. In several samples with neuropathology, we observed large concretions crisscrossed by deep, jagged fractures leading to partial or total cleavage within calcified conglomerates. In the parenchyma, we detected wide pinealocyte-free fluid-filled areas adjacent to the calcified zones. Our findings demonstrate the dynamic nature of PG calcification that provides new insights into the formation of PG concretions in normal aging and neurodegenerative diseases.

2 | MATERIALS AND METHODS

2.1 | Sample description

Thirty-two PGs tissue samples, $6 \times 7 \times 7$ mm³ in media dimension each, with different extents of calcification were taken from postmortem human brains. Fifteen samples were PGs in normal aging without neurodegenerative pathology (34–95-year old), 6 with VD pathology (66–80-year old), and 11 with AD pathology (65–92-year old). Table S1 in Supplementary materials reports the description of the samples, including its name as well as gender and age.

The study was carried out on autopsy material obtained from the collection of Federal State Scientific Institution Research Institute of Human Morphology (Moscow, Russian Federation). All protocols were approved by the Ethical Committee of the Research Institute of Human Morphology of the Russian Academy of Medical Sciences (now FSSI Research Institute of Human Morphology) (No. 6A of 19 October 2009) and are in correspondence with instructions of the Declaration of Helsinki, including points 7–10 for human material from 12.01.1996 with the last amendments from 19.12.2016.

2.2 | Sample preparation for X-ray tomographic, histological, and immunohistochemical image acquisition

The samples fixed in formalin or Carnoy fluid were measured via X-ray micro-CT in air without paraffin embedding. Next, the PGs were dehydrated in eight portions isopropyl alcohol and embedded in cylindrical paraffin blocks $7 \times 7 \times 10$ mm³ dimension, as for routine histological examination, and were measured via micro-CT and XPCT.

After the X-ray experiments, the samples were prepared for histological and immunohistochemical analysis. Paraffin blocks were cut at 6- μ m thickness sections and stained with Mallory-method for connective tissue or gallocyanine for the visualization of cell nuclei. Immunohistochemical staining with GFAP-antibodies (dilution 1:1000, Thermo Fisher Scientific) was used for the identification of glial tissue. These sections were examined microscopically to identify areas within the blocks that contained histological features of interest—namely, pinealocytes, connective and glial tissue, and concretions. The Zeiss A1, made in Germany, a light compound microscope was used for the microscopic measurement.

2.3 | Experimental setup

Micro-computed tomography (micro-CT): Laboratory-based micro-CT was used to select and evaluate

samples of PGs with different degrees of pineal calcification. Micro-CT experiments were carried out using the laboratory microtomography setup TOMAS (Federal Scientific Research Center “Crystallography and Photonics” RAS). Micro-CT image contrast is generated due to different absorptions of X-ray radiation by structures of the investigated object having different electron densities. The accelerating voltage and current were 45 kV and 40 mA, respectively. X-ray beam energy was 17.5 keV (pyrographite crystal was used as a monochromator). In each tomographic scan, 1000 X-ray projected images were acquired in an angular range of 200 degrees with a step of 0.5 degrees. The experiments were carried out with a parallel beam geometry. The scan time for the whole sample was about 100 min. The XIMEA xiRAY11 detector had a pixel size of $9 \times 9 \mu\text{m}^2$.³⁰

X-ray phase-contrast tomography: Detailed high-resolution 3D images of some samples selected by micro-CT were produced using synchrotron-based XPCT. This imaging technique is sensitive to small density variations in weakly absorbing objects. We used PBI XPCT technique that exploits image contrast formation via free wave propagation between sample and detector (the overview of X-ray phase-contrast imaging and tomography techniques, as well as related references, can be found in Ref. [31]).

The XPCT scans of the samples of PGs in normal aging, AD, and VD pathology were performed at the SYRMEP beamline of the Elettra Synchrotron, Trieste, Italy. The samples were scanned using a white (polychromatic) X-ray beam with a mean energy of 21.5 keV. Si filter of 1.5 mm was used for filtering the energy spectrum. Each sample was scanned with a setup resulting in acquired images having an effective pixel size of $3 \times 3 \mu\text{m}^2$ and also with a setup capable of imaging a region of interest (ROI) within each sample resulting in acquired images with an effective pixel size of $0.9 \times 0.9 \mu\text{m}^2$. During a stepwise tomographic scan, we acquired 1800 projections with rotation of the sample over 180 degrees. The detector exposure time for each projection was 250 ms. The sample-to-detector distance was 50 cm for the low-resolution (i.e., $3 \times 3 \mu\text{m}^2$) scans and 15 cm for the high-resolution (i.e., $0.9 \times 0.9 \mu\text{m}^2$) scans. We measured each sample with two vertical steps in low-resolution and 4–5 vertical steps in high-resolution scans.

The samples of PGs in normal aging and AD pathology were measured in a series of experiments at the P05 beamline of the synchrotron facility PETRA III, DESY, operated by the Helmholtz-Zentrum Hereon (PETRA III, DESY).³² A double crystal monochromator (Si111) was used to produce a monochromatic beam. In the first experiment, the X-ray energy was about 25 keV. The tomography was acquired in extended field of view (eFOV)³³ with 4000 projections and an exposure time of 0.25 s, covering a total angle range of 360 degrees.

The sample was placed at a distance—50 cm from the recording system with pixel sizes $0.64 \times 0.64 \mu\text{m}^2$. In the second experiment, a monochromatic beam energy of 30 keV was used. As the sample dimensions exceeded the beam size, the tomography was acquired in an eFOV setup, and three FOVs with 3 mm distance from each other were measured for each sample. A total of 9003 projections were taken for each FOV covering a total angle range of 360 degrees. Exposure time was 500 ms. The sample was placed at a distance of 25 cm from the recording system. Each projection image was acquired with magnification 10 \times , resulting in an effective pixel size $0.64 \times 0.64 \mu\text{m}^2$. The detector has 5120×3840 pixels, but an ROI in vertical direction was used to cut off unusable parts of the image. Thus, each sample was scanned with 4–5 vertical steps.

2.4 | Image reconstruction procedure

The tomographic reconstruction of micro-CT data was performed with the CGLS algebraic method.^{34,35} Morphometric analysis of the micro-CT reconstructed images was done with the Python-based workflow for ad-hoc data analysis developed at Federal Research Center “Crystallography and Photonics” RAS, Moscow. A preliminary median filtration of 3D micro-CT images was performed before virtual segmentation of the sample. The subsequent segmentation of the PG as well as the calcium concretions was carried out using global threshold binarization. In Table S1, the total sample volume (TV) and calcified concretions volume (CV) parameters were calculated by counting voxels of binarized images.

XPCT data preprocessing, phase, and tomographic reconstructions were performed using the open-source software toolkit SYRMEP Tomo Project^{36,37} and MATLAB package.³⁸ Each X-ray projected image was pre-processed via dark field and flat field corrections and a ring removal Raven filter.³⁹ The algorithm based on Paganin equation⁴⁰ and the reconstruction pipeline³⁸ were applied to the preprocessed projections to retrieve the phase shift information. Filtered Back Projection with a linear ramp filter was used for tomographic reconstruction. Grayscale variations in reconstructed tomography images represent changes in absorption coefficient (absorption contrast) or electron density (phase contrast).

Average intensity projection (“Z Project” tool of ImageJ/Fiji) through tomographic volume with a thickness of $6 \mu\text{m}$ was used to match histological sections that in routine have about $6\text{-}\mu\text{m}$ thickness. Image processing and data visualization were performed using standard tools and plugins of the open-source program ImageJ/Fiji⁴¹ and Ref. [42]. The average diameter of concretions was estimated using distance-transform methods described in Ref. [43].

2.5 | Statistical analysis

Micro-CT image-based statistical analysis was carried out by means of the software Statistica, version 12. Normal distributions of data were proved by the Kolmogorov–Smirnov normality test. The data were analyzed using the Kruskal–Wallis test for non-normally distributed values. Differences were considered statistically significant at $p < 0.05$ for all statistical tests.

3 | RESULTS

3.1 | Micro-CT experiments

Figure 1a shows a photographic image of the sagittal section of the postmortem human brain. The red arrow shows the location of PG in the epithalamus, near the center of the brain. Figure 1b displays the image of PG (with habenula visible at the top of the figure). Figure 1c illustrates 3D tomographic image of PG. The PG in the figure contains many aggregated and non-aggregated concretions of different sizes and shapes. High absorbing calcifications are visible in white.

We classified the calcified deposits in 32 samples (15 PGs in normal aging, 11 PGs with AD, and 6 PGs with VD) based on their location in the PG. The result is shown in Figure 2. The figure provides the name of the samples, neurological status of PG donors, topological arrangement of calcified zones, and cysts.

In Table S1, we have reported detailed description the samples shown in Figure 2, including PGs morphometric characteristics of each PG obtained via micro-CT (see description in Section 2): TV—total sample volume, mm^3 , CV—concretions volume, mm^3 , CV/TV—percentage of concretions in the total volume of the sample, %.

Results of the statistical analysis (see the description of the method in Section 2) based on morphometric parameters listed in Table S1 are shown in Figure 3.

The box plots in Figure 3 show (a) the total volume (TV), (b) CV, and (c) degree of pineal calcification (CV/TV) of PGs in normal aging and PGs with neurodegenerative pathology. As we notice some outlier values in samples with neuropathology are remarkably larger than the average value. PG volume in VD is on average noticeably smaller when compared with PG in normal aging. No significant correlations between the degree of pineal calcification and neurological status are observed. This result is consistent with Vigh et al.¹⁹

3.2 | XPCT experiments: the normal PG

The XPCT images were used to study in detail the micromorphology of PGs. Images in Figure 4 illustrate typical PG tissue in natural aging. Grayscale XPCT slice

image of PG is shown in Figure 4a. The region/tissue of interest was selected to illustrate both calcified deposits (bottom right) and soft tissue (rest of the PG tissue surrounding the deposits). The gray level in the figure is adjusted to show both parenchyma and calcified tissue. The calcified region shown in the figure is a collection of both non-aggregated and aggregated concretions. A large-scale calcified conglomerate shown with the white arrow was formed due to the coalescence of several concretions independently developed from the primary centers of their formation. Free space between the incompletely fused concretions is well visible in Figure 4a. This calcified conglomerate was observed in the inner part of the parenchyma.

Figure 4b shows the zoom of the XPCT image highlighting the region of parenchyma with fibrovascular stroma (yellow arrow), blood vessels (red arrow), and pinealocytes (cyan arrows). Figure 4c presents the XPCT image of the parenchyma arranged in lobules. Figure 4d shows the image, obtained via immunohistochemical staining of PG with GFAP-antibodies to detect glial fibers, corresponding to the image in Figure 4c. The lobular pattern is well visible in both figures. To assess the micromorphological features of the parenchyma and reach information on the arrangement and state of parenchyma cells in the XPCT images, we performed virtual segmentation of the cells. The result of the segmentation is shown in Figure 4e. PG cells and their processes are marked in purple, and blood vessels are marked in yellow. Figure 4f illustrates the histological section (Mallory staining) of the sample with morphological features similar to the reconstructed XPCT slice in Figure 4e. Clusters of the pinealocytes, glial cells and their processes, and the blood vessels surrounded by glial fibers are well distinguishable in both parts (f) and (e) of Figure 4. Via XPCT, we identified in some samples single and multiple cysts surrounded by PG parenchymal tissue with a fibrous structure composed of glial cells processes replacing pinealocytes in cystic lesions (for more information about PG cysts, see Ref. [29]).

3.3 | Pineal gland in old-age, VD pathology, and AD disease (XPCT imaging)

The results and summary of the XPCT research conducted on the PG samples in normal aging and pathological conditions are presented here in Figures 1–7 and in Figures S1–S9. Both PGs with and without neuropathology showed a wide variety of shapes and types of concretions. Concretions located in the pial capsule (extrapineal location) and inside the parenchyma (intrapineal location) were common findings in each group of PGs. In some specimens, the intrapineal concretions were absent. In each group we observed both laminated and nonlaminated calcified concretions. In

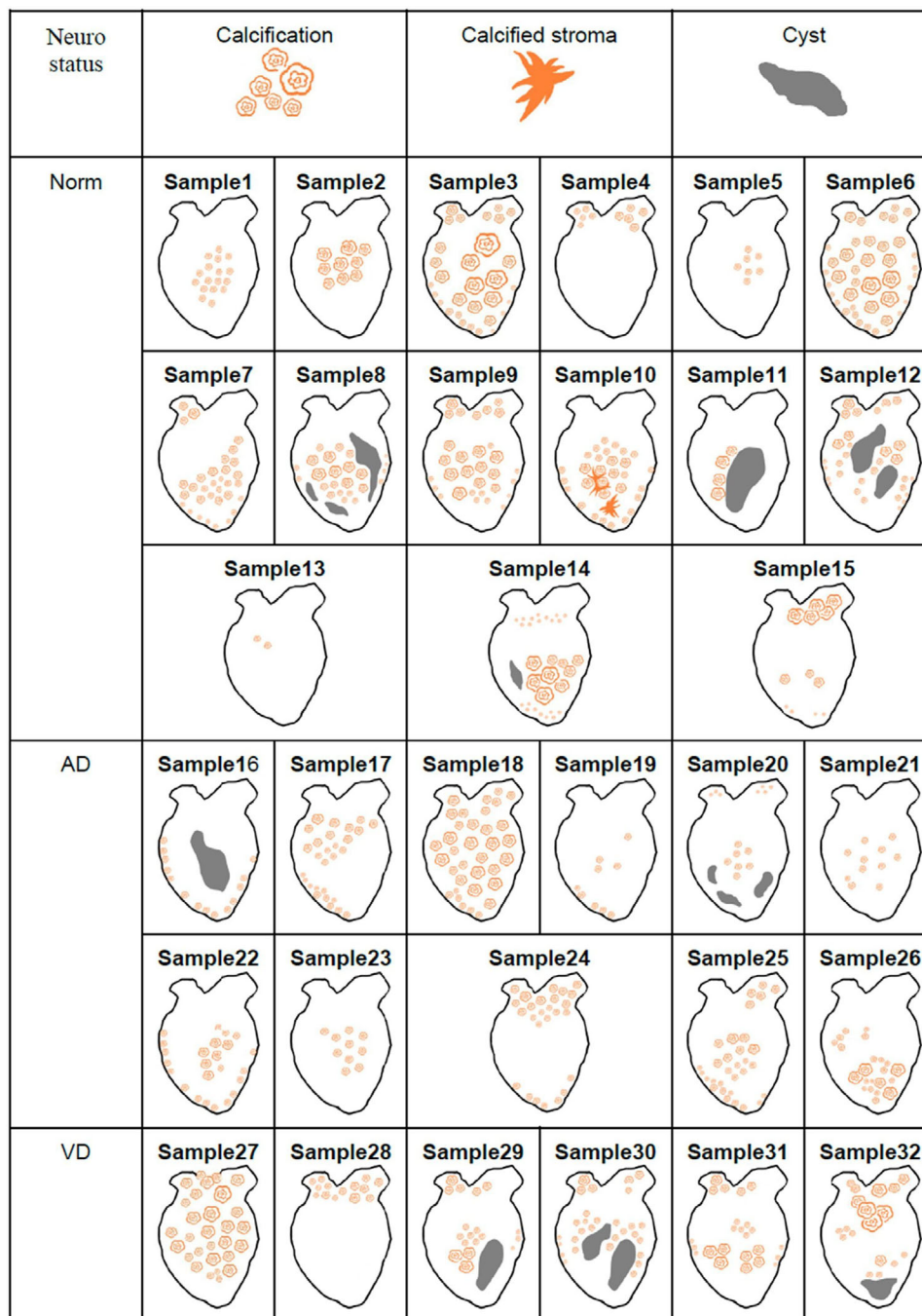


FIGURE 2 Location of calcified zones and cysts in PGs

addition, in some specimens we find mulberry-like conglomerates formed of numerous agglomerated nodes. The aggregation of multiple concretions in some cases caused large-scale lamination on the whole conglomerate. Additionally, we observed micro-granules with irregular shapes scattered in PG parenchyma. Separate concretions reached a dimension of hundred microns. Aggregated concretions formed calcified conglomerate with the size of up to several mm. In some specimens, stroma and vessels were calcified. The results are in agreement with the micro-CT, CT

experiments, and with previously published scientific reports.^{4,26,44–46}

XPCT imaging revealed high-resolution details of age-related PG alteration. In particular, PG concretions of PGs from 2 elderly donors aged 81 and 82, showed evidence of moderate destruction. In specimens with neuropathologies, we observed the noticeable degeneration process such as segregation of concretions from PG calcified aggregates, hollow core in non-aggregated concretions, and high segregation of layers in concretions with concentric lamination structure. In some

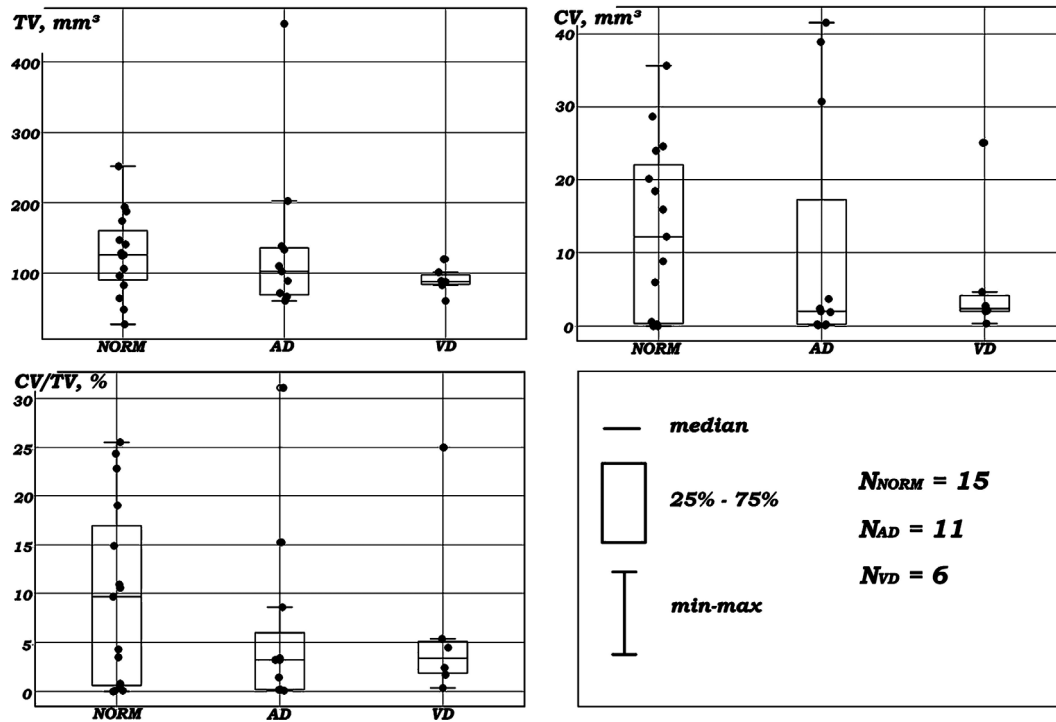


FIGURE 3 Box plots showing the variation of PGs morphometric characteristics within PGs in normal aging, and PGs with AD and VD pathologies: (top left) TV—total volume of the sample, mm³; (top right) CV—concrements volume, mm³; (bottom left) CV/TV—percentage of concrements in the total PG volume, %; (bottom right) legend and number of samples per group

of AD and VD specimens, we observed well-marked numerous large deep cracks passed through the whole PG concrements.

Figure 5 illustrates examples of intrapineal calcified deposits that can occur in both neuropathology (a–d) and old-age (e and f). Parts (a) and (b) of Figure 5 show, respectively, an XPCT slice and histological section (Mallory staining) of a concrement surrounded by pinealocytes. Figure 5c presents XPCT slice image of multiple concrements with concentric lamination. The concrements aggregated together to form a larger concrement. In the center of concrement formation, a dense granule (visible in white) was observed. Similar granules were found in different samples with and without neuropathology (see white spots in Figure 5c,e, respectively). The origin of the granules is unknown and requires further research. Figure 5d illustrates the aggregation of concrements independently developed from primary centers of their formation and the detachment of concrements.

Damage of concrements may also be present in normal PG. The analysis of PGs without neuropathology showed moderate signs of concrements destruction in two elderly donors. Figure 5e,f illustrates detachment of layers within concrements and the partial splitting of concrements, respectively. However, we observed that PGs in neuropathology, compared with normal PGs, typically show more pronounced degenerative abnor-

malities such as hollow nuclei, highly segregated layers, and deep cracks.

Figure 6a shows a grayscale XPCT image of the concrement in VD pathology with concentric lamination structure of alternating light (denser) and dark (less dense) layers. The layered concrement developed from the single primary centers, started to disintegrate with the segregation of denser layers. The arrow indicates the internal links remaining after the segregation. Figure 6b presents a concentric concrement with a hollow core in VD pathology. The arrow points the indicative signs of the detachment on the internal surface of the hollow concrement. Figure 6c illustrates a calcified conglomerate in VD sample traversed by a deep, jagged fissure that caused the laminated concrement inside to be completely fragmented.

Moreover, in the sample with AD pathology, the involution of PG calcification has a distinct character (see Figure 6d–f). The AD sample, shown in Figure 6d, contains heavily degraded concrements with segregated layers and a hollow core. Concrements in Figure 6e,f have numerous large deep cracks. The evident sign of PG degeneration indicates that apparently, the formation of PG calcification in neurodegenerative diseases is a dynamic process characterized by the development and destruction of calcified PG zones.

In our XPCT research, we were particularly interested in studying PG soft tissue adjacent to the calcified

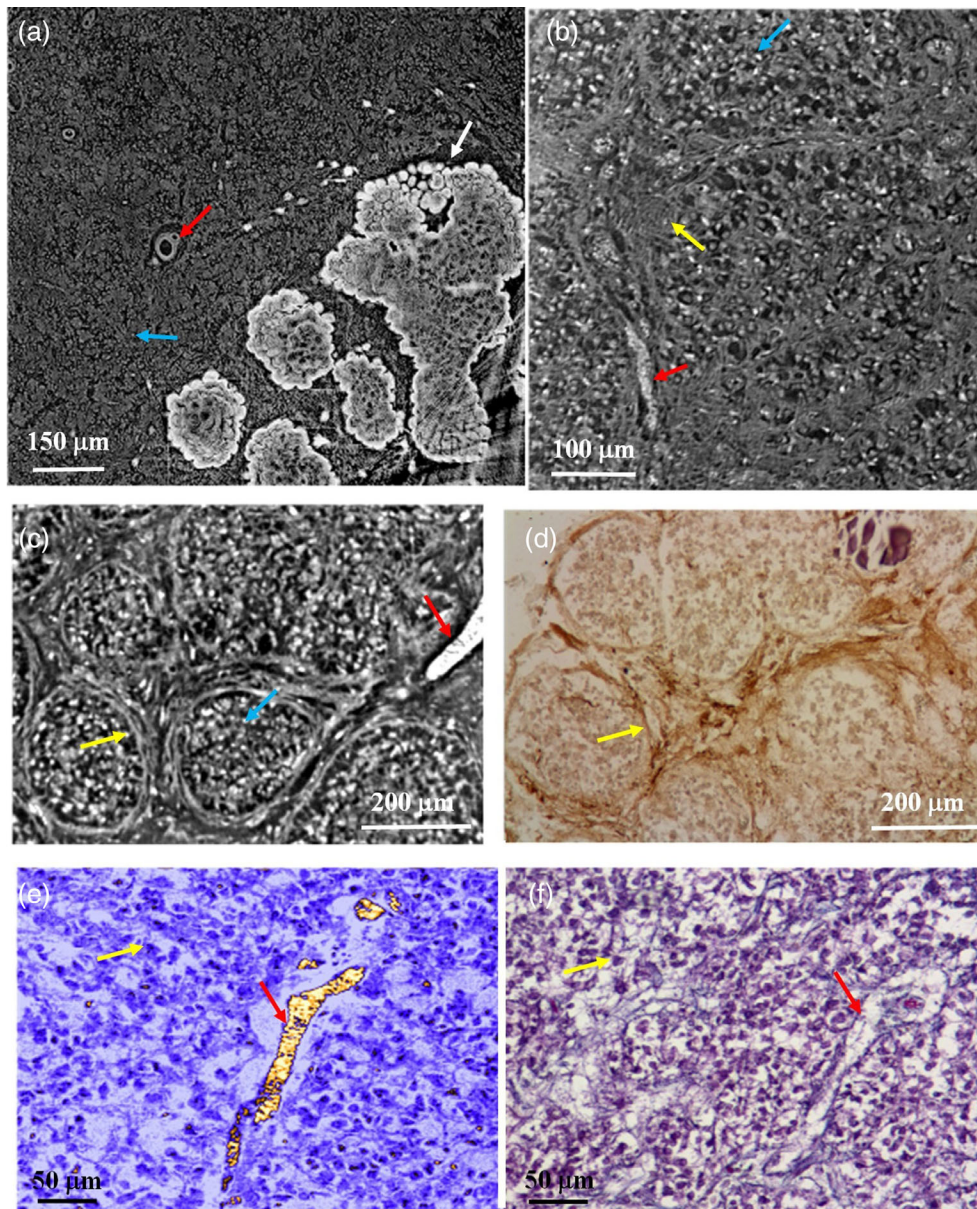


FIGURE 4 Typical PG in normal aging: (a) XPCT image of PG tissue with PG concretions (white arrow) at the bottom right of the figure. Blood vessels (red arrow) and nuclei of pinealocytes (white spots marked with the cyan arrow) are visible in parenchyma; (b) zoom of the XPCT image highlighting the region of parenchyma with fibrovascular stroma (yellow arrow), blood vessels (red arrow), and pinealocytes (cyan arrow); (c) PG parenchyma arranged in lobules (XPCT image): pinealocytes (cyan arrows) and glial fibers (yellow arrow); (d) immunohistochemical staining with GFAP-antibodies glial fibers showing the lobular structure corresponding to (c); (e) XPCT image with the virtual segmentation of pinealocytes (purple) and blood vessels (yellow); (f) histological section (Mallory staining) of PG parenchyma with morphological features similar to the XPCT image (e). (a and b) SYRMEP ELETTRA experiment, voxel size = $0.9 \times 0.9 \times 0.9 \mu\text{m}^3$. (c and e) PETRA III, DESY experiment, voxel size = $0.64 \times 0.64 \times 0.64 \mu\text{m}^3$

zones. Figure 7a,b shows XPCT slices of PG in AD and VD pathologies, respectively. The concretions in the figures are mulberry-like conglomerates with numerous interconnected nodes. One can see a hollow core and segregation of layers in concretions. In the PG parenchyma of samples with neurodegeneration, wide pinealocyte-free fluid-filled areas were detected around concretions (Figure 7). In some AD samples (not shown here), we observed concretions surrounded by an outer layer of connective tissue.

Figure 7c illustrates the histological section (Mallory staining) of the PG corresponding to Figure 7b.

4 | DISCUSSION

In the present study, we observed a wide variability of pineal morphology, including the shape and size of the PG, the structure of PG parenchyma and stroma, as well as the topological arrangement and texture

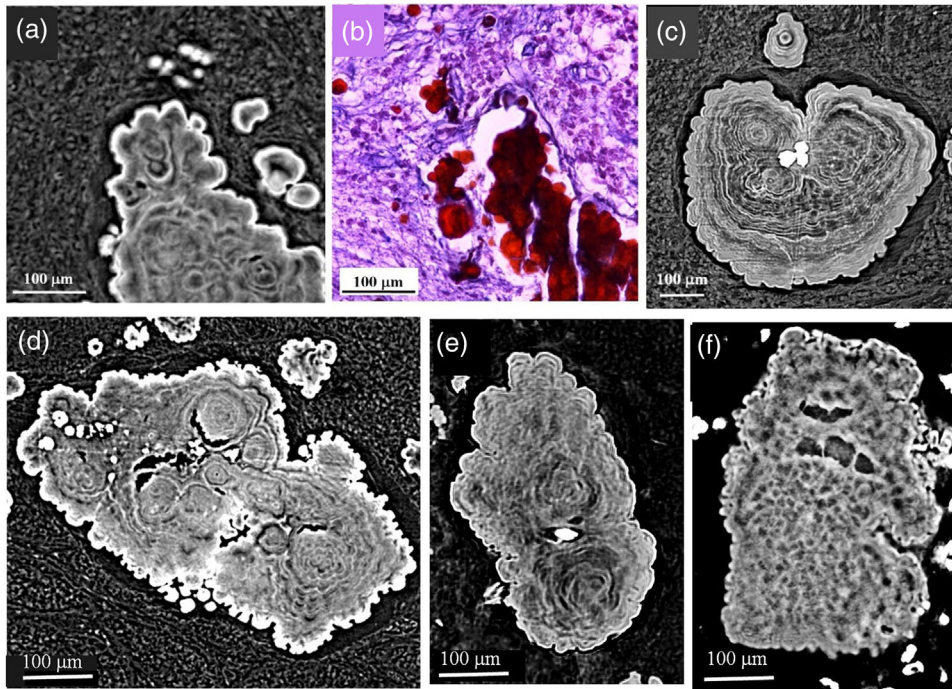


FIGURE 5 XPCCT image of PG with V pathology (a, c, d), and PG from old donor without neuropathology (e and f): (a) concretion surrounded by pinealocytes; (b) histological section (Mallory staining) of PG with VD; (c) two concretions with concentric lamination aggregated together to form a larger concretion; (d) aggregation of multiple concretions with well visible segregation some of them; (e) detachment of layers within concretions; (f) the partial splitting of concretion. SYRMEP ELETTRA experiment, voxel size $0.9 \times 0.9 \times 0.9 \mu\text{m}^3$

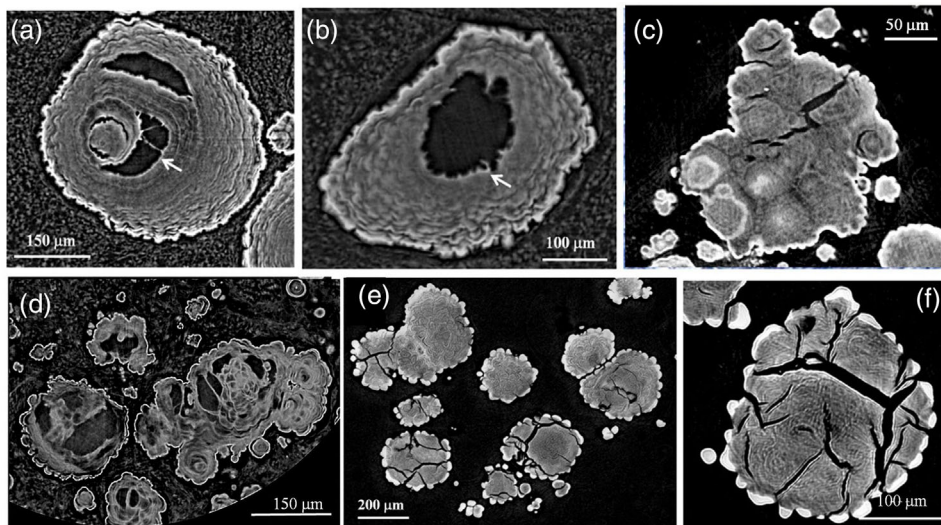


FIGURE 6 Grayscale XPCCT slice image. (a–c) VD group: (a) concretion with segregation of layers. The arrow indicates the internal links remaining after the segregation; (b) concretion with a hollow core. The arrow indicates characteristic irregularities on the surface of the concretion; (c) calcified conglomerate traversed by a deep, jagged fissure; (d–f) AD group: (d) concretions with segregation of layers and hollow core; (e) concretions with numerous large cracks; (f) zoom of a concretion with cracks. (a–d) SYRMEP ELETTRA experiment, voxel size $0.9 \times 0.9 \times 0.9 \mu\text{m}^3$; (e and f) PETRA III, DESY experiment, voxel $0.64 \times 0.64 \times 0.64 \mu\text{m}^3$

of calcium deposits. The prevalence of pineal calcification in each group was either single deposits with or without laminar structure or mulberry-like calcified conglomerates with large numbers of concretions. In many samples, we observed the coexistence of

several types of concretions. Occasionally calcified deposits were absent in some specimens of each group. We did not observe a correlation between morphometric parameters of PG and the neuropathological state of the pineal organ. This is likely to

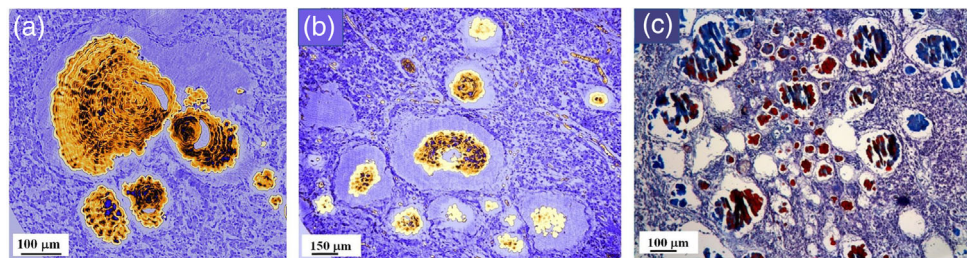


FIGURE 7 PG parenchyma and concrements in samples with neurodegeneration. (a and b) XPCT slice of AD (a) and VD (b) samples. Parenchyma is colored purple, concrements are yellow; (c) histological section (Mallory staining) of the PG corresponding to (b). In (a and b), holes in the concretions and pinealocyte-free fluid-filled areas of the soft tissue adjacent to concretions are clearly visible.

be because of a limited number of samples under investigation.

In literature, the correlation of PG calcification with aging and neurodegenerative disorders is still controversial. It has been generally said that calcified deposits in human PGs, correlate positively with aging, and that their amount might be associated with a variety of neurological diseases.⁵ Currently, it was reported a strong association of PG calcification with AD. The degree of PG calcification in AD patients was higher compared with controls and patients with other types of dementia.¹⁵ On the other hand, the authors of Ref. [27] reported the opposite results, that is, fewer concretions have been found in PG in patients with AD. Moreover, studies^{46–48} reported that in their research on PG neither pineal weight nor calcium deposition showed changes in AD. In addition, the PGs of AD patients, cells, or afferent fibers were clear from neuropathological hallmarks of AD, that is, neurofibrillary tangles, the accumulation of neurofilaments, tau, hyperphosphorylated tau, or beta/A4 amyloid deposition.⁴⁹ Despite the numerous studies on the calcification of the PG in AD, research of PG concretions in VD patients is underrepresented in scientific literature.

The possible reasons for these inconsistencies in literature might be a prominent individual variability of the pineal organ and different degrees of calcification among nations and populations living in different time zones.^{50–55} On the other hand, the ambivalent findings might be related to the limited capabilities of ordinary research techniques.

The advanced XPCT imaging technique we used in this research enabled 3D visualization of the whole unstained PG with micro-features of the parenchyma and calcification, which could not be seen with other imaging tools. The most important finding of our XPCT-based investigation is the detection of degenerative process in concretions and parenchyma of PGs with neurological pathology. In particular, we observed the considerable segregation of concretions from calcified mulberry-like conglomerates. In addition, we detected a hollow core and highly segregated layers in concretion with lamination structure. Moreover, we found

numerous deep cracks passing through the PG concretions with lamination structure. In the parenchyma of the samples with neurodegeneration, we detected wide pinealocyte-free fluid-filled areas adjacent to the calcified zones. We found in AD concretions surrounded by an outer layer of the glial fibers and partly of fibroblast replaced the pinealocytes. Similar findings previously have been reported by Saveliev et al. in the case of schizophrenia.⁵⁶ They suspected the process of active calcium exchange between the calcifications and the surrounding tissues. In their opinion, pathological processes can accelerate the dissolution of the concretions. The nature of this process is still unclear.

To the best of our knowledge, no one has observed in 3D a degeneration of concretions or examined in deep the parenchyma next to concretions in AD and VD. Well-established imaging techniques such as histological and immunohistochemical methods as well as transmission and scanning electron microscopy have a limited capability due to invasive sample preparation (in particular, for the visualization of PG parenchyma with large concretions). On the other hand, PG researches with noninvasive imaging such as X-ray microtomography, MRI, and XPCT previously have been limited by either spatial resolution of image (MRI), low sensibility to soft tissue visualization (micro-CT),²⁷ or by the object of study (XPCT, PG in aging).^{4,29}

The process of PG calcification has been known and studied for a long time, but the genesis and dynamics of PG concretions are not yet well understood. Before our research, the prevalence of publication on PG calcification dynamics was dedicated to the process of PG formation; no studies have investigated the destruction of concretions. Several mechanisms possibly responsible for the development of calcification in PG of different species have been proposed in Refs. [25, 57–61]. Both components, including pineal cells and collagen fibers, are thought to be involved in these processes. Our research indicates that, apparently, the PG calcification formation is a dynamic process characterized by both the development and destruction of calcified PG zones. To complement the current results, XPCT

could be combined with structural techniques such as X-ray diffraction imaging.⁶²

In our research, we indicated two ways of PG calcification degeneration possibly correlated with neurodegenerative diseases. The analyzed data reported in this study will be an important resource for further investigation of PG morphology and the mechanism of formation and degeneration of concretions in aging and neuropathology.

This study deals with the micromorphology of PG, and it did not address the issue of melatonin. However, because melatonin as an antioxidant and neuroprotector may contribute to the pathogenesis of AD and VD, it would be interesting to study in future research the correlation of morphology and dynamics of PG calcifications to the production of melatonin.

In this research, XPCT was helpful in detecting the PG degeneration processes. As future perspective, additional extensive studies may be carried out over a larger set of samples per group (control, AD, VD).

5 | CONCLUSIONS

XPCT in-deep investigation of the PG micromorphological features revealed the evident signs of degeneration in PG concretions and parenchymal tissue adjacent to calcified zones in AD and VD samples. We indicated several ways of PG concretions destruction. Particularly, we observed a hollow core and highly segregated layers in laminated concretions, as well as numerous deep cracks passing through the PG calcified deposits. Our scientific finding indicates that PG calcification is a dynamic process characterized by the development and destruction of calcified zones. Moreover, we observed large pinealocyte-free fluid-filled regions surrounding calcified zones that had not been detectable with other imaging techniques. Our research provides a basis for the future study of PG involvement in neurodegeneration and enriches the knowledge about PG in the normal and pathological state.

ACKNOWLEDGMENTS

The bilateral project CNR/RFBR (2018–2020)—accordo CNR-RFBR delle Relazioni Internazionali (CUP B86C17000210005 and Russian number 18-52-7819), the national project RFBR (number 18-29-26028)—Russian Federation, The FISR Project “Tecnopolo di nanotecnologia e fotonica per la medicina di precisione” (funded by MIUR/CNR, CUP B83B17000010001) and the TECNOMED project (funded by Regione Puglia, CUP B84I18000540002) are acknowledged for financial support of the experiments. Ministry of Science and Higher Education within the State assignment FSRC “Crystallography and Photonics” RAS in part of carrying out experiments.

CONFLICT OF INTEREST

The authors have no conflicts to disclose.

DATA AVAILABILITY STATEMENT

The data that support the findings of this study are available on request from the corresponding author.

REFERENCES

1. Erlich SS, Apuzzo MLJ. The pineal gland: anatomy, physiology, and clinical significance. *J Neurosurg*. 1985;63(3):321-341. <https://doi.org/10.3171/jns.1985.63.3.0321>
2. Bocchi G, Valdre G, Valdre G. Physical, chemical, and mineralogical characterization of carbonate-hydroxyapatite concretions of the human pineal gland. *J Inorg Biochem*. 1993;49(3):209-220. [https://doi.org/10.1016/0162-0134\(93\)80006-U](https://doi.org/10.1016/0162-0134(93)80006-U)
3. Baconnier S, Lang SB, Polomska M, Hilczer B, Berkovic G, Meshulam G. Calcite microcrystals in the pineal gland of the human brain: first physical and chemical studies. *Bioelectromagnetics*. 2002;23(7):488-495. <https://doi.org/10.1002/bem.10053>
4. Kim J, Kim HW, Chang S, Kim JW, Je JH, Rhyu IJ. Growth patterns for acervuli in human pineal gland. *Sci Rep*. 2012;2(984):1-5. <https://doi.org/10.1038/srep00984>
5. Tan DX, Xu B, Zhou X, Reiter RJ. Pineal calcification, melatonin production, aging, associated health consequences and rejuvenation of the pineal gland. *Molecules*. 2018;23(2):301. <https://doi.org/10.3390/molecules23020301>
6. Hasegawa A, Ohtsubo K, Mori W. Pineal gland in old age; quantitative and qualitative morphological study of 168 human autopsy cases. *Brain Res*. 1987;409(2):343-349. [https://doi.org/10.1016/0006-8993\(87\)90720-7](https://doi.org/10.1016/0006-8993(87)90720-7)
7. Trufakin VA, Shurygina AV. The problems of the central regulation of immune system biorhythms: the role of exogenous and endogenous melatonin. *Vestn Ross Akad Med Nauk*. 2006;(9-10):121-127. Russian.
8. Ljubicić D, Stipcević T, Pivac N, Jakovljević M, Mück-Seler D. The influence of daylight exposure on platelet 5-HT levels in patients with major depression and schizophrenia. *J Photochem Photobiol B*. 2007;89(2-3):63-69. <https://doi.org/10.1016/j.jphotobiol.2007.09.002>. Epub 2007 Sep 19.
9. Maślińska D, Laure-Kamionowska M, Deręgowski K, Maśliński S. Association of mast cells with calcification in the human pineal gland. *Folia Neuropathol*. 2010;48(4):276-282.
10. Tapp E, Huxley M. The histological appearance of the human pineal gland from puberty to old age. *J Pathol*. 1972;108(2):137-144. <https://doi.org/10.1002/path.1711080207>
11. Champney TH, Joshi BN, Vaughan MK, Reiter RJ. Superior cervical ganglionectomy results in the loss of pineal concretions in the adult male gerbil (*Meriones unguiculatus*). *Anat Rec*. 1985;211(4):465-468. <https://doi.org/10.1002/ar.1092110414>
12. Groves WC, Brandt J, Steinberg M, Warren A, Rosenblatt A, Baker A, Lyketsos CG. Vascular dementia and Alzheimer's disease: is there a difference? A comparison of symptoms by disease duration. *J Neuropsychiatry Clin Neurosci*. 2000 Summer;12(3):305-315. <https://doi.org/10.1176/jnp.12.3.305>
13. Rizzi L, Rosset I, Roriz-Cruz M. Global epidemiology of dementia: Alzheimer's and vascular types. *Biomed Res Int*. 2014;2014:908915. <https://doi.org/10.1155/2014/908915>. Epub 2014 Jun 25.
14. Humbert W, Pévet P. Calcium content and concretions of pineal glands of young and old rats. A scanning and X-ray microanalytical study. *Cell Tissue Res*. 1991;263(3):593-596. <https://doi.org/10.1007/BF00327294>
15. Mahlberg R, Walther S, Kalus P, et al. Pineal calcification in Alzheimer's disease: an in vivo study using computed

- tomography. *Neurobiol Aging*. 2008;29(2):203-209. <https://doi.org/10.1016/j.neurobiolaging.2006.10.003>. Epub 2006 Nov 13.
16. Korczyn AD, Vakhapova V, Grinberg LT. Vascular dementia. *J Neurol Sci*. 2012;322(1-2):2-10. <https://doi.org/10.1016/j.jns.2012.03.027>. Epub 2012 May 8.
 17. Korczyn AD. Mixed dementia—the most common cause of dementia. *Ann N Y Acad Sci*. 2002;977:129-134. <https://doi.org/10.1111/j.1749-6632.2002.tb04807.x>
 18. Doyle AJ, Anderson GD. Physiologic calcification of the pineal gland in children on computed tomography: prevalence, observer reliability and association with choroid plexus calcification. *Acad Radiol*. 2006;13(7):822-826. <https://doi.org/10.1016/j.acra.2006.04.004>
 19. Vigh B, Szél A, Debreceni K, Fejér Z, Manzano e Silva MJ, Vigh-Teichmann I. Comparative histology of pineal calcification. *Histol Histopathol*. 1998;13(3):851-870. <https://doi.org/10.14670/HH-13.851>
 20. Kunz D, Schmitz S, Mahlberg R, Mohr A, Stöter C, Wolf KJ, Herrmann WM. A new concept for melatonin deficit: on pineal calcification and melatonin excretion. *Neuropsychopharmacology*. 1999;21(6):765-772. [https://doi.org/10.1016/S0893-133X\(99\)00069-X](https://doi.org/10.1016/S0893-133X(99)00069-X)
 21. Mahlberg R, Kienast T, Hädel S, Heidenreich JO, Schmitz S, Kunz D. Degree of pineal calcification (DOC) is associated with polysomnographic sleep measures in primary insomnia patients. *Sleep Med*. 2009;10(4):439-445. <https://doi.org/10.1016/j.sleep.2008.05.003>. Epub 2008 Aug 27.
 22. Sandyk R. Pineal and habenula calcification in schizophrenia. *Int J Neurosci*. 1992;67(1-4):19-30. <https://doi.org/10.3109/00207459208994773>
 23. Humbert W, Pévet P. Permeability of the pineal gland of the rat to lanthanum: significance of dark pinealocytes. *J Pineal Res*. 1992;12(2):84-88. <https://doi.org/10.1111/j.1600-079x.1992.tb00031.x>
 24. Bulc M, Lewczuk B, Prusik M, Gugolek A, Przybylska-Gornowicz B. Calcium concretions in the pineal gland of the Arctic fox (*Vulpes lagopus*) and their relationship to pinealocytes, glial cells and type I and III collagen fibers. *Pol J Vet Sci*. 2010;13(2):269-278.
 25. Przybylska-Gornowicz B, Lewczuk B, Prusik M, Bulc M. Pineal concretions in turkey (*Meleagris gallopavo*) as a result of collagen-mediated calcification. *Histol Histopathol*. 2009;24(4):407-415. <https://doi.org/10.14670/HH-24.407>
 26. Krstić R. A combined scanning and transmission electron microscopic study and electron probe microanalysis of human pineal acervuli. *Cell Tissue Res*. 1976;174(1):129-137. <https://doi.org/10.1007/BF00222155>
 27. Fokin EI, Savelyev SV, Gulimova VI, Asadchikov EV, Senin RA, Buzmakov AV. The morphogenesis and spatial organization of human epiphyseal concretions in Alzheimer's disease, schizophrenia, and alcoholism. *Arkh Patol*. 2006;68(5):20-22.
 28. Bravin A, Coan P, Suortti P. X-ray phase-contrast imaging: from pre-clinical applications towards clinics. *Phys Med Biol*. 2013;58(1):R1-35. <https://doi.org/10.1088/0031-9155/58/1/R1>. Epub 2012 Dec 10.
 29. Bukreeva I, Junemann O, Cedola A, et al. Investigation of the human pineal gland 3D organization by X-ray phase contrast tomography. *J Struct Biol*. 2020;212(3):107659. <https://doi.org/10.1016/j.jsb.2020.107659>. Epub 2020 Oct 24.
 30. Buzmakov AV, Asadchikov VE, Zolotov DA, et al. Laboratory microtomographs: design and data processing algorithms. *Crystallogr Rep*. 2018;63:1057-1061. <https://doi.org/10.1134/S106377451806007XM4>
 31. Mayo S., Endrizzi M. X-ray phase contrast methods. In: Ida N, Meyendorf N, eds. *Handbook of Advanced Non-Destructive Evaluation*. Springer; 2018:1-42. https://doi.org/10.1007/978-3-319-30050-4_54-1
 32. Wilde F, Ogurreck M, Greving I, et al. Micro-CT at the imaging beamline P05 at PETRA III. AIP Conference Proceedings. American Institute of Physics Inc.; 2016:030035. <https://doi.org/10.1063/1.4952858>
 33. Vo NT, Atwood RC, Drakopoulos M, Connolley T. Data processing methods and data acquisition for samples larger than the field of view in parallel-beam tomography. *Opt Express*. 2021;29(12):17849-17874. <https://doi.org/10.1364/OE.418448>
 34. Buzmakov A, Nikolaev D, Chukalina M, Schaefer G. Efficient and effective regularised ART for computed tomography. *Annu Int Conf IEEE Eng Med Biol Soc*. 2011;2011:6200-6203. <https://doi.org/10.1109/IEMBS.2011.6091531>
 35. Chukalina MV, Ingacheva AS, Buzmakov AV, Krivososov YS, Asadchikov VE, Nikolaev DP. A hardware and software system for tomographic research: reconstruction via regularization. *Bull Russ Acad Sci: Phys*. 2019;83(2):150-154.
 36. Brun F, Massimi L, Fratini M, et al. SYRMEP Tomo Project: a graphical user interface for customizing CT reconstruction workflows. *Adv Struct Chem Imaging*. 2017;3(1):4. <https://doi.org/10.1186/s40679-016-0036-8>. Epub 2017 Jan 19.
 37. van Aarle W, Palenstijn WJ, De Beenhouwer J, et al. The ASTRA Toolbox: a platform for advanced algorithm development in electron tomography. *Ultramicroscopy*. 2015;157:35-47. <https://doi.org/10.1016/j.ultramicro.2015.05.002>. Epub 2015 May 6.
 38. Moosmann J, Ershov A, Weinhardt V, et al. Time-lapse X-ray phase-contrast microtomography for in vivo imaging and analysis of morphogenesis. *Nat Protoc*. 2014;9(2):294-304. <https://doi.org/10.1038/nprot.2014.033>. Epub 2014 Jan 9.
 39. Raven C. Numerical removal of ring artifacts in microtomography. *Am Inst Phys*. 1998;69(8):2978-2980. <https://doi.org/10.1063/1.1149043>
 40. Paganin D, Mayo SC, Gureyev TE, Miller PR, Wilkins SW. Simultaneous phase and amplitude extraction from a single defocused image of a homogeneous object. *J Microsc*. 2002;206(pt 1):33-40. <https://doi.org/10.1046/j.1365-2818.2002.01010.x>
 41. Schindelin J, Arganda-Carreras I, Frise E, et al. Fiji: an open-source platform for biological-image analysis. *Nat Methods*. 2012;9:676-682. <https://doi.org/10.1038/nmeth.2019> PMID: 22743772
 42. Gómez-de-Mariscal E, García-López-de-Haro C, Ouyang W, Donati L, Lundberg E, Unser M, Muñoz-Barrutia A, Sage D. Deep-ImageJ: A user-friendly environment to run deep learning models in ImageJ. *Nat Methods*. 2021;18(10):1192-1195. <https://doi.org/10.1038/s41592-021-01262-9> PMID: 34594030
 43. Hildebrand T, Rügsegger P. A new method for the model independent assessment of thickness in three-dimensional images. *J Microsc*. 1997;185:67-75. <https://doi.org/10.1046/j.1365-2818.1997.1340694.x>
 44. Zimmerman RA, Bilaniuk LT. Age-related incidence of pineal calcification detected by computed tomography. *Radiology*. 1982;142(3):659-662. <https://doi.org/10.1148/radiology.142.3.7063680>
 45. Scharenberg K, Liss L. The histologic structure of the human pineal body. *Prog Brain Res*. 1965;10:193-217. [https://doi.org/10.1016/s0079-6123\(08\)63452-4](https://doi.org/10.1016/s0079-6123(08)63452-4)
 46. Wu YH, Swaab DF. The human pineal gland and melatonin in aging and Alzheimer's disease. *J Pineal Res*. 2005;38:145-152. <https://doi.org/10.1111/j.1600-079X.2004.00196.x>
 47. Friedland RP, Luxenberg JS, Koss E. A quantitative study of intracranial calcification in dementia of the Alzheimer type. *Int Psychogeriatr*. 1990 Spring;2(1):36-43.
 48. Wu YH, Swaab DF. The human pineal gland and melatonin in aging and Alzheimer's disease. *J Pineal Res*. 2005;38:145-152. <https://doi.org/10.1111/j.1600-079X.2004.00196.x>
 49. Pardo CA, Martin LJ, Troncoso JC, Price DL. The human pineal gland in aging and Alzheimer's disease: patterns of cytoskeletal antigen immunoreactivity. *Acta Neuropathol*. 1990;80(5):535-540. <https://doi.org/10.1007/BF00294615>

50. Adeloje A, Felson B. Incidence of normal pineal gland calcification in skull roentgenograms of black and white Americans. *Am J Roentgenol Radium Ther Nucl Med*. 1974;122(3):503-507. <https://doi.org/10.2214/ajr.122.3.503>
51. Bhatti IH, Khan A. Pineal calcification. *J Pak Med Assoc*. 1977;27(4):310-312.
52. Chiba M, Yamada M. About the calcification of the pineal gland in the Japanese. *Psychol Clin Neurosci*. 1948;2(4):301-303. <https://doi.org/10.1111/j.1440-1819.1948.tb02770.x>
53. Daramola GF, Olowu AO. Physiological and radiological implications of a low incidence of pineal calcification in Nigeria. *Neuroendocrinology*. 1972;9(1):41-57. <https://doi.org/10.1159/000122036>
54. Mugondi SG, Poltera AA. Pineal gland calcification (PGC) in Ugandans. A radiological study of 200 isolated pineal glands. *Br J Radiol*. 1976;49(583):594-599. <https://doi.org/10.1259/0007-1285-49-583-594>
55. Fan KJ. Pineal calcification among black patients. *J Natl Med Assoc*. 1983;75(8):765-769.
56. Saveliev SV, Erofeeva EA, Fokin EI, Gulimova VI, de Klerk N, Postnov AA. Human Epiphyseal concrements in schizophrenia. *Arkh Patol*. 2004;4:13-16.
57. Vigh B, Szél A, Debreceni K, Fejér Z, Manzano e Silva MJ, Vigh-Teichmann I. Comparative histology of pineal calcification. *Histol Histopathol*. 1998;13(3):851-870. <https://doi.org/10.14670/HH-13.851>
58. Welsh MG. Pineal calcification: structural and functional aspects. *Pineal Res Rev*. 1985;3:41-68.
59. Krstić R. Ultracytochemical localization of calcium in the superficial pineal gland of the Mongolian gerbil. *J Pineal Res*. 1985;2(1):21-37. <https://doi.org/10.1111/j.1600-079x.1985.tb00625.x>
60. Krstić R. Pineal calcification: its mechanism and significance. *J Neural Transm Suppl*. 1986;21:415-432.
61. Vigh-Teichmann I, Vigh B. Immunocytochemistry and calcium cytochemistry of the mammalian pineal organ: a comparison with retina and submammalian pineal organs. *Microsc Res Tech*. 1992;21(3):227-241. <https://doi.org/10.1002/jemt.1070210306>
62. Cedola A, Mastrogiacomo M, Lagomarsino S, et al. Orientation of mineral crystals by collagen fibers during in vivo bone engineering: an X-ray diffraction imaging study. *Spectrochim Acta, B*. 2007;62(6-7):642-647. <https://doi.org/10.1016/j.sab.2007.02.015> ISSN 0584-8547

SUPPORTING INFORMATION

Additional supporting information can be found online in the Supporting Information section at the end of this article.

How to cite this article: Bukreeva I, Junemann O, Cedola A, et al. Micromorphology of pineal gland calcification in age-related neurodegenerative diseases. *Med Phys*. 2023;50:1601–1613. <https://doi.org/10.1002/mp.16080>